Stipčević Josip (Orcid ID: 0000-0002-1419-4892)

Molinari Irene (Orcid ID: 0000-0002-8314-1444)

Dasović Iva (Orcid ID: 0000-0003-4017-9271)

Crustal thickness beneath the Dinarides and surrounding areas from receiver functions

Josip Stipčević[1], Marijan Herak[1], Irene Molinari[2], Iva Dasović[1], Hrvoje Tkalčić[3], Andrej Gosar[4,5]

[1]Department of Geophysics, Faculty of Science, University of Zagreb, Zagreb, Croatia.
[2]Istituto Nazionale di Geofisica e Vulcanologia, Sezione di Bologna, Italy.
[3]Research School of Earth Sciences, The Australian National University, ACT 0200, Australia.
[4]Slovenian Environment Agency, Ljubljana, Slovenia.
[5]University of Ljubljana, Faculty of Natural Sciences and Engineering, Ljubljana, Slovenia.

Corresponding authors: Josip Stipčević (jstipcevic@gfz.hr), Marijan Herak (herak@irb.hr)

Abstract

Knowledge about the crustal thickness is one of the key elements in the reconstruction of the regional tectonic history. The Dinaric mountain belt is one of the most enigmatic segments of the Alpine-Mediterranean collision zone, characterized by large variations in crustal thickness and not studied sufficiently. We present a new Moho depth map for the wider Dinarides region which was created using teleseismic earthquake recordings from 87 permanent and temporary seismic stations in the region. Teleseismic data were analyzed using the receiver function method to extract converted P to S waves.

This article has been accepted for publication and undergone full peer review but has not been through the copyediting, typesetting, pagination and proofreading process which may lead to differences between this version and the Version of Record. Please cite this article as doi: 10.1029/2019TC005872

The resulting Moho topography fits well within a structural framework comprising a thicker crust under the Dinarides, which gradually becomes thinner towards the Pannonian and Adriatic domains. The profiles crossing the north-western Dinarides are marked by a relatively sharp decrease in crustal thickness north of the main thrust front. This transition is followed by significant crustal thinning towards the Pannonian basin. The Mohorovičić discontinuity lies the deepest in the central and southern Dinarides, at depths of over 55 km. Here, similarly to the north-western segment we observe a jump in the crustal thickness when transitioning towards the Internal Dinarides, which hints at possible underthrusting (or subduction) of the Adria plate in this region. Moho depths in the transition zone towards the Pannonian basin and in the Pannonian basin proper vary between 25 and 35 km. In the Adriatic domain we find crustal thickness ranging from 30 km to more than 45 km around the Central Adriatic islands.

Keywords: Mohorovičić discontinuity, crustal thickness, Dinarides, Adriatic microplate, receiver functions

Key points:

- New crustal thickness map of the Dinarides and surrounding areas
- Thicker crust in the central Adriatic, a deep crustal root in the south Dinarides and a tightly constrained transition from the deep Dinaric to the shallower Pannonian Moho
- Jump in the crustal thickness when transitioning towards the Internal Dinarides, which hints at possible underthrusting of the Adria plate in this region

1. Introduction

The eastern Adriatic margin, where the Adriatic microplate (Adria) is subducted beneath Eurasia to form the Dinaric mountain belt, is one of the most enigmatic segments of the Alpine-Mediterranean collision zone. Subduction in this area began in the Middle Jurassic with the closing of Neotethyan ocean and lasted until Late Cretaceous–early Paleogene time (Pamić, 2002; Schmid et al., 2008; Ustaszewski et al., 2010) when it was replaced by collision involving nappe stacking and folding. Thrusting gradually migrated from northeast to southwest into the external part of the orogen thus leading to the formation of the external Dinarides fold-thrust belt (Fig. 1). While the thrusting process in the External Dinarides continued undisturbed the Internal Dinarides came under the influence of the extension processes connected with the opening of the Pannonian Basin in the Middle Miocene (Horváth et al., 2006; Matenco & Radivojević, 2012; Ustaszewski et al., 2010). The Pannonian Basin was created in response to the northward movement of Adria which caused lateral extrusion from the Alpine region which in turn initiated rapid rollback of a slab attached to the European continent (Ratschbacher et al., 1991a,b; Horváth, 1993; Horváth et al., 2006; Ustaszewski et al., 2008; van Gelder et al. 2017). Extension in the Pannonian region was accompanied by thinning of the lithosphere and influx of the hotter material from the asthenosphere (Ustaszewski et al., 2010; Matenco & Radivojević, 2012; Handy et al., 2014). After cessation of the extension processes in the Late Miocene the Internal Dinarides were once again exposed to the contraction due to the translation and counterclockwise rotation of Adria. At present, the Adria–Europe convergence is still ongoing across the eastern Adriatic-Dinarides region and it is mostly accommodated by thrusting and strike-slip faulting within the external Dinarides (van Unen et al., 2018 and references therein).

The seismicity of the region is mainly concentrated along the Adria–Dinarides collision zone (Fig. 1), and the Alps–Dinarides contact region, but significant earthquakes have also occurred in the broad transitional zone between the Alps, the Dinarides and the Pannonian basin, within the Internal Dinarides, and in the central part of the Adria. The foci are practically all shallow, within the upper crust (Herak et al., 1996, updated until April 2018).

This brief outline clearly shows the complexity surrounding the formation of Dinaric mountains and emphasizes the need to further investigate processes involved. And while the general image is not disputed, there are numerous open questions on past and current processes connected with the creation of the Dinarides. For example, is there a slab gap in the Northwestern and Central Dinarides (Bijwaard & Spakman, 2000; Piromallo & Morelli, 2003; Koulakov et al., 2009; Šumanovac & Dudjak, 2016; Šumanovac et al., 2017; Subašić et al., 2017, Belinić et al., 2018), and if so, why? Is the subduction still active in the southern Adriatic (Bennett et al., 2008)? Furthermore, deciphering the tectonic evolution of the Dinarides is not only significant in the local

context but is one of the key elements in understanding of how the central Mediterranean evolved through interaction of Adriatic microplate and the Eurasian mainland. Adriatic microplate plays the crucial role in the formation of the central Mediterranean (Handy et al., 2015) and any new insight may have profound influence on our understanding of tectonics in the Mediterranean basin. Characterizing the depth to the Mohorovičić discontinuity is essential in reconstructing the tectonic past of an area. Compared to the close neighbours, such as the Alps and the Apennines, the Dinarides are comparatively poorly researched and only a handful of seismological studies have only recently started to deal with deep crust and transition to mantle here using data from rapidly growing local seismic networks (*e.g.* Stipčević et al., 2011; Šumanovac et al., 2016, 2017; Subašić et al., 2017; Belinić et al., 2018; Kapuralić et al., 2019). In particular, no concentrated effort has been made to update the only map of the Moho topography in the greater Dinarides area by Aljinović et al. (1987) and Skoko et al. (1987) (see below) published over 32 years ago. In the meantime, several European projects aiming at mapping the Moho covered the Dinarides too (*e.g.* Grad et al., 2009; EPcrust model by Molinari & Morelli, 2011) but with insufficient resolution and detail to be used in mapping local features of interest. For these reasons we have concentrated our efforts on providing the first-order estimates of crustal thickness underneath the Dinarides, thus improving the knowledge about the crust in the area and possibly sheding light on the interaction between the Adria and the European mainland. In order to do this, we have used available data from the permanent and temporary stations in the wider Dinarides region (Fig. 2; see also below) in conjunction with the receiver function analyses.

2. Earth structure under the Dinarides

The crustal structure under the Dinarides is generally still poorly resolved. It is dominated by large seismic transition zones that are not obviously linked to the tectonic structures observed at the surface (Aljinović, 1983; Herak & Herak, 1995; Šumanovac, 2010; Stipčević et al., 2011, Kapuralić et al. 2019). Most of our general knowledge about the deep crustal structure under the Dinarides stems from the large seismic refraction/reflection surveys conducted in the period 1964–1983 (Dragašević, 1969, 1973–1974; Dragašević & Andrić, 1975; Skoko et al., 1987). Aljinović (1983) mapped two strong refractors: one shallow, which was interpreted as the boundary between the sedimentary cover and the crystalline basement and a significantly deeper one ascribed to the Mohorovičić discontinuity. Interpolating the results of deep seismic sounding experiments mentioned above Aljinović et al. (1987) and Skoko et al. (1987) published the first map of the Moho topography in this wider area, showing a relatively narrow belt of thicker crust (>40km) following the main axis of the Dinarides and thinning rapidly towards the Pannonian basin and the Adriatic Sea.

More recently, active seismic exploration was performed on three profiles (Alp01, Alp02 and Alp07) in the north-western Dinarides and south-western edge of the Pannonian basin as a part of the larger Alp 2002 experiment in the Eastern Alps

(Brückl et al., 2007; Šumanovac et al., 2009). The results confirmed a general scheme of two layered crust with thickest crust under the Dinarides decreasing from about 40 km in the NW Dinarides to 25 km in the Pannonian basin and 30 km in the Adriatic. Extending the research to central and southern Dinarides Šumanovac (2010) used results from the Alp07 profile to calibrate two-dimensional modelling of gravity data. The results of this modelling established transitional zone between Dinaric and Pannonian crust and suggested a deep seated Dinaric crustal root with very sharp transition to more shallow crust on the northern edge. This sharp transition was interpreted as the main fault at the Moho level where Adriatic microplate underthrusts Europe. Receiver function studies done in several regions of the area qualitatively confirmed the model with thick crust under Dinarides (van der Meijde et al., 2003; Stipčević et al., 2011; Orešković et al., 2011, Šumanovac et al., 2016). Receiver function probing also revealed significantly thicker crust in the central-southern external Dinarides than previously thought. Both van der Meijde et al. (2003) and Stipčević et al. (2011) estimated crust thickness in excess of 45 km beneath the islands of the central Adriatic while the second study also mapped thickness exceeding 50 km under some of the inland stations.

The deeper structures of the Dinaric collision zone have only recently been considered using local data. Global and regional scale seismic tomography studies indicated an inclined high-velocity zone down to a depth of around 160 km beneath the central-southern Dinarides (Bijwaard & Spakman, 2000; Piromallo & Morelli, 2003; Koulakov et al., 2009; Zhu et al., 2012). This anomaly has been interpreted as subducted Adriatic lithosphere (Wortel & Spakman, 2000) located west of the presumed Adria-Eurasia plate boundary that is marked by an oceanic suture zone (Ustaszewski et al., 2010). Large scale tomographic models of the area show an unusual feature, a large low-velocity anomaly beneath the northern Dinarides that separates the aforementioned slab anomaly in the southern Dinarides from the slab anomaly beneath the Eastern Alps (but see Šumanovac & Dudjak, 2017, with a contrasting view). To explain this slab gap Ustaszewski et al. (2008) suggested that the slab was thermally eroded due to opening of the Pannonian basin and influx of asthenospheric material, which is indirectly supported by the observation that fast axis determined by SKS-splitting analyses here are oriented perpendicularly to the Adriatic coast and mountain chains (Subašić et al., 2017). Handy et al. (2015) built on this idea and incorporated slab tearing beneath Dinarides and subsequent rise of the asthenosphere as the crucial mechanism in the explanation of the slab gap. Matenco & Radivojević (2012) suggested that at least part of the extension in the south-eastern Pannonian basin and Internal Dinarides is caused by the lithospheric delamination under the Dinarides. Delamination may have progressed further into the External Dinarides and this would have profound influence on how we see the geodynamical process in the area.

3. Data

The data set used to compute P-wave receiver functions (PRFs) consists of more than 21000 waveform sets consisting of 3 component seismograms, from teleseismic events with Mw ≥ 5.5 at epicentral distances between 30° and 100°. The waveforms were recorded at 87 permanent broadband stations from regional networks, run by the Department of Geophysics, University of Zagreb and the Croatian Seismological Survey (network code CR), the Slovenian Environment Agency (SL), the Montenegro Seismological Observatory (ME), the Seismological Survey of Serbia (SJ), and the Kövesligethy Radó Seismological Observatory (Hungary, HU). In addition, we also included stations belonging to the MedNet (MN, MedNet project partner institutions, 1988), as well as to the AlpArray (Z3, Hetényi et al., 2018; Molinari et al., 2016) and AlpArray-CASE (8X, Molinari et al., 2018) temporary networks. Station coverage (Figure 2) is the densest along the coast and in the northwestern part of the study area (Slovenia and NW Croatia). It is the sparsest in the central and eastern Bosnia and Herzegovina. The basic station parameters are presented in the table in the Supplement.

Number of waveforms per station varied depending on the station operational time. For some stations we acquired more than 300 recordings, while for some recently installed stations we were able to acquire only several tens of usable teleseismic seismograms. All the waveforms were visually checked and recordings without clear P-wave arrival were discarded. This resulted in approximately 13,000 high quality records which were then used to calculate receiver functions.

4. Receiver function method

Since its inception in the late 1970s, the receiver function method (Langston, 1977; Vinnik, 1977) has become one of the most used tools in the crustal and upper mantle exploration. It is conceptually a fairly simple approach and consists of isolating the effects of mode conversions generated at impedance contrasts bellow the seismic station. Receiver functions can be generated from both P and S teleseismic waves (Yuan et al., 2006) but due to the higher frequency content the P-wave receiver functions are usually used in the imaging of the crust. PRFs are created by steeply impinging teleseismic P-waves that get converted to S waves at local velocity contrast and due to this most of the information about local structure is recorded on horizontal components. To isolate effects of the local structure the vertical component is deconvolved from the horizontal ones (Langston, 1979; Ammon, 1991). Calculation of receiver functions starts with rotation of the waveforms to the RTZ coordinate system, where R is the radial direction along the great circle path from the epicenter to the station, T is the transverse direction perpendicular to R in the horizontal plane, and Z is the vertical component. In the next step we discard traces without clear P-wave arrival and use iterative time-domain deconvolution (Ligorrıa & Ammon, 1999) with a frequency cut off at 1.0 Hz to calculate receiver functions. In the end, we visually

inspect all the receiver functions at each station and discard low quality ones using signal to noise ratio as the main criterion of quality.

4.1. H–κ stacking

In the analysis of the receiver functions we follow an approach of *H*–*κ* stacking (Zandt & Ammon, 1995; Chevrot & van der Hilst, 2000; Zhu & Kanamori, 2000) to retrieve the average crustal properties beneath each station. *H*–*κ* technique utilizes Moho converted *Ps* and reverberated PpPs and PpSs+PsPs phase arrival times in a grid search directed stacking. Grid search goes over *H* (Moho depth) and *κ* (*Vp/Vs*) values, calculates phase arrival times and computes A_{ij} as the stack of weighted values of the observed PRFs at those times for the *i*-th *H* and *j*-th *κ*. The best estimates of crustal thickness and the *Vp/Vs* ratio are taken to correspond to the maximum of the summation. Grid search is done under the assumption of one layered crust and known *P* wave velocity. As some of the phases are more pronounced, appropriate weights are assigned to each phase. In our case standard values used by Zhu & Kanamori (2000) of 0.7-0.2-0.1 were selected for Ps, PpPs and PpSs + PsPs phase stacks. Lombardi et al. (2008) suggest using equal weights to ensure equal phase importance but we choose less weighting on latter arriving phases to suppress arrival time ambiguity present when the Moho interface has a dip. A trade-off between *H* and *κ* is always present, and it is further enhanced when a differential weighting is used. To minimize this trade-off we have used the modified *H*–*κ* stacking (Chen et al., 2010), which relies on calculating the coherence between the P-to-S conversions and the reverberation phases at different *κ* values. *H*–*κ* search was performed for an average P-wave crustal velocity value of *Vp* = 6.2 km/s, based on studies by Herak & Herak (1995) and Šumanovac et al. (2009). Epistemic uncertainty of the depth introduced by lateral variation of the average crustal *Vp* value is generally small, and does not exceed ± 5% for realistic crustal *Vp* values. Basic *H*–*κ* search domain was set in the range of 20–70 km for crustal thickness and 1.65–1.90 for *Vp/Vs* but minimal allowed *H* varied depending on the tectonic province the stations belong to (Fig. 2, see below).

Apart from the inherent trade-off between *H* and *Vp/Vs* the main sources of error when using *H*–*κ* technique to explore young orogenic areas, such as the Dinarides, are the assumptions of flat, non-dipping Moho interface, and the one of a single-layered, isotropic crust. Grad & Tiira (2012) give an overview of other possible sources of error in *H*–*κ* analyses, and Lombardi et al. (2008) use synthetic PRFs to warn of overestimation of *H* by the *H*–*κ* method for dipping interfaces. Li et al. (2019) peformed a thorough analysis of the adverse impact that Moho dip and crustal anisotropy have on estimated *H* and *κ*, and Ogden et al. (2019) also analyse the considerable influence of gradational Moho, heterogenous crust, and the choice of processing parameters on the final results. In our case, one of the important possible ambiguities stems from multilayered crust. While this is not a problem for stations in the Pannonian Basin (Figs. 2–4) where crust can mostly be approximated by a single layer (*e.g.* Šumanovac et al., 2009), in the Dinarides strong impedance contrasts are found at the bottom of carbonates at the depths of about 5–15 km (*e.g.* Aljinović,

1983), and/or at the Conrad discontinuity (typically at depths of 25–35 km). This may pose problems for the H–κ algorithm, as the conversions from intracrustal discontinuities arrive before those coming from the Moho, and may be of a comparable amplitude (see Fig. 3 and H–κ stack for station PDG in Fig. 4).

In the case of stations CRES (Fig. 3b, Fig. 4) situated in the Pannonian Basin, and BBLS (Fig. 3a, Fig. 4) in the Internal Dinarides domain, Moho P-to-S conversion (Ps) is easy to identify as the first and the strongest arrival after P, although for station CRES there is a Moho depth ambiguity due to the several strong reverberating phases (Fig. 4). However, for the stations CA06A/B (the station CA06A on the island of Palagruža was moved to a new location 82 m away where its code became CA06B, so we merged recordings into one stack), CA09A, PDG, and DUGI (Fig. 3c–f) a phase is clearly seen in the stack before the one we identify as the Moho conversion based on the proximity of its arrival time and the theoretical arrival times for a reasonable range of Moho depths. For instance, for the station DUGI (Figs. 2, 3f) the two strong phases marked in the figure arrive 2.3 and 5.8 s after the first P. Previous study by van der Meijde et al. (2003) indicates Moho to be about 41 km deep there, and the most recent available Moho map by Molinari & Morelli (2011) suggests depth of about 37 km. For κ =1.85, Vp = 6.2 km/s, these depths correspond to the delay of the Ps phase of 5.0–5.5 s after the first arrival of P-wave. Hence, the second phase is interpreted as Ps conversion from the Moho. Similar reasoning holds for the station CA06A/B (Fig. 3c), but here the phase we interpret as the Moho-related Ps is actually weaker than the preceding one, and an automatic procedure would erroneously assign too shallow Moho there. This can be even more clearly seen from the H–κ stack results for station A253A (Fig. 4). The results show two pronounced stack maxima with the automatically picked maximum having unreasonably low crustal thickness and κ values. Our preferred results are marked with the yellow stars in the Fig. 4.

We have therefore defined the lower threshold for allowed values of H to different levels for the three groups of stations shown in Fig. 2. The Moho depth in the Pannonian Basin was not restricted, for stations within the belt of External Dinarides the Moho was not allowed shallower than 40 km, and elsewhere H > 25 km was imposed.

5. Application of the method and results

The H–κ procedure performed as described above for all considered stations yielded the sets of triplets $T_{ijk} = (H_{ik}, \kappa_{jk}, A_{ijk})$, where H_{ik} is the i-th considered crustal thickness, κ_{jk} is the j-th considered κ, and A_{ijk} is the corresponding value of stacked amplitudes, all for the k-th station. The estimated depth to the Mohorovičić discontinuity and the Vp/Vs ratio below the k-th station (H_k, κ_k) are then simply the values of H_{ik} and κ_{jk} corresponding to the maximum of A_{ijk}. The confidence regions of the best solution may

be estimated following Rychert & Harmon (2016), by assuming that the region around the maximum of A_{ijk} approximates the likelihood function with a normal distribution (Draper & Smith, 1998). Then the surface A_{ijk} is proportional to exp(–E), E being the variance surface between the prediction and observations. The surface A_{ijk} is next transformed so as to make it proportional to the variance:

$$E \sim -\ln(A_{ijk}) + 1/snr. \quad (1)$$

As the A_{ijk} is normalized so that its maximum is equal to one (implying min(E) = 0.0), the inverse of the estimate of signal-to-noise ratio, $1/snr$, is added as the measure of the minimal possible variance. Because the condition snr > 4.0 was used in the analyses, we conservatively assume the representative value of snr = 6.0. The estimate of α-level confidence regions where $E < E_\alpha$ for the k-th station is then computed using the inverse F-distribution (F_{inv}) as suggested by Draper & Smith (1998):

$$E_\alpha(H, \kappa) = E(H_k, \kappa_k)[1 + n \,/\, (d - n)\, F_{inv}(n, d - n, \alpha)], \quad (2)$$

where n is the number of parameters (n = 2), and d is the number of receiver functions observed at that station. The α-confidence intervals for H_k, and κ_k are defined as

$$CI_{H,k,\alpha} = \pm\{\max[H_{ik}(E < E_\alpha)] - \min[H_{ik}(E < E_\alpha)]\}/2\ , \quad (3)$$

$$CI_{\kappa,k,\alpha} = \pm\{\max[\kappa_{jk}(E < E_\alpha)] - \min[\kappa_{jk}(E < E_\alpha)]\}/2\ .$$

The confidence intervals (3) are used to define the relative station quality, q_k, to be proportional to the inverse sum of confidence intervals for H_k and κ_k normalized by their span over all stations:

$$q_k \propto \{CI_{H,k,\alpha}\,/[CI_{H,\alpha,max} - CI_{H,\alpha,min}] + CI_{\kappa,k,\alpha}\,/[CI_{\kappa,\alpha,max} - CI_{\kappa,\alpha,min}]\}^{-1}. \quad (4)$$

The individual vales of H_{ik} and κ_{jk} are shown in the maps in Figs. 5 and 6 by colour-coding of the corresponding station symbols. The symbol size scales with the station quality factor q_k. The table in the Electronic Supplement presents estimated H_k and κ_k for each station, along with their confidence limits and quality factors q_k.

In order to map the inferred Moho topography, instead of using some interpolant between the best individual estimates of H, we have interpolated the values of A_{ijk} onto a regular grid of 8.3 × 8.3 km. For a grid cell centered at geographical coordinates (φ, λ), 2-D array $A_{ij\varphi\lambda}$ is found as the spatial weighted average of all A_{ijk} that are closer to the cell than some maximum correlation distance D_{max}. The weights are set to be proportional to the inverse squared station–cell distance D_k and to the station quality factor q_k:

$$A_{ij\varphi\lambda} = \sum_k w_k A_{ijk}(D_k < D_{max}) \,/\sum_k w_k\,, \quad w_k = q_k/(20 + D_k^2), \quad D_{max} = 50 \text{ km}. \tag{5}$$

The representative value of $H_{\phi\lambda}$ (the crustal thickness below the cell centered at φ, λ) is then the one corresponding to the maximum of the $A_{ij\phi\lambda}$. The resulting depths were subsequently smoothed with a spatial kernel of the radius of 41.5 km (5 grid cells), to produce the Moho topography map shown in Fig. 5.

The confidence intervals $CI_{H\varphi\lambda}$ for $H_{\phi\lambda}$, and $CI_{\kappa\varphi\lambda}$ for $\kappa_{\phi\lambda}$ in each grid cell were assessed as described above for each individual measurement, replacing A_{ijk} with $A_{ij\phi\lambda}$ from (5), and using the weighted mean of the number of contributing receiver functions, $N_{\phi\lambda}$, instead of n in (2). The gridded values $H_{\phi\lambda}$, $CI_{H\varphi\lambda}$, $\kappa_{\phi\lambda}$, and $CI_{\kappa\varphi\lambda}$ are available from the respective tables in the Electronic Supplement.

Figure 5 shows the map of the interpolated Moho depth values and associated uncertainties obtained from the expression (5). Although the map shows strong variation in crustal thickness (from 25 to 55 km) the results are consistent within the various tectonic domains. There are two distinct zones, the Adriatic-Dinarides zone with deeper Moho (>40 km) and much shallower one in the Internal Dinarides-Pannonian zone (Fig. 5a,c) where the crustal thickness varies between 25 and 35 km. High values of crustal thickness is the feature that can be traced under the entirety of the External Dinarides extending to some degree into to the region of the Adriatic Sea. Quality of the H–κ stacking results at each of the stations (circle sizes in Fig. 5) is generally good with the exception of stations in the areas with the complex Earth structure. These stations are mainly located in the External Dinarides where strong crustal discontinuities obscure or interfere with the signal from the deeper Moho interface, which is reflected in the uncertainty estimation (Fig. 5b). In a recent paper Li et al. (2019) warn that in the areas where Moho dip is considerable (as is the case here), and/or anisotropy is not negligible, application of traditional H–κ may produce biased results. Likewise, Ogden et al. (2019) showed that gradational Moho, as well as complicated crustal structure, will also have adverse effect on the accuracy and confidence of results. The largest uncertainty in Moho depth estimates (>5 km) can be seen in the Central and Southern Dinarides (Fig. 5b) where the combination of limestone cover, thick crust, interface inclination and deep reflectors all combine to create large lateral variation in the Moho depth estimate. However, even for these areas we find that consistent Moho estimates are retrieved. This is mostly due to the good station coverage with at least several neighboring stations producing similar results.

Simultaneously with the extraction of the crustal thickness we obtained *Vp/Vs* values and using the procedure described above created average crustal *Vp/Vs* map shown

in Fig. 6. Contrary to the crustal thickness results, *Vp/Vs* ratio varies significantly throughout the region. The results range from rather low values (1.60–1.65) to very high values of 1.95, with an average of 1.77. The variation of *Vp/Vs* ratio is significant even for some neighboring stations and this strong lateral change is clearly visible in the uncertainty map (Fig. 6b). The causes of this variation are many but the main one is high sensitivity of *Vp/Vs* values to small variations in the $H-\kappa$ stack values. As shown by Lombardi et al. (2008) smearing of the $H-\kappa$ stack maximum is mainly caused by the complex crustal structure (dipping interfaces, strong crustal discontinuities, etc.) and this influences the stability of the results (see their Figures 6 and 7). Furthermore, Li et al. (2019) caution about the influence of P-wave crustal anisotropy, which may cause apparent low values of *Vp/Vs* with little influence on the Moho depth. Whereas the Moho depth values are relatively stable and change predictably, the variation in *Vp/Vs* values can be high even for small changes in crustal structure. This is especially true in the regions with highly fractured limestone cover where variation in *Vs* between layers can be large depending on fluid content inside the layers. The higher *Vp/Vs* uncertainty can be clearly seen in the examples shown in Figure 4. This effect is actually exacerbated in the areas with thinner crust (compare stations CRES and PDG in Figure 4).

6. Discussion and conclusions

As can be seen from Moho depth compilations shown in Figs. 7a and 7b a number of previous studies have mapped strongly variable crustal thickness in the wider Dinarides region. These compilations are based on the results from deep seismic refraction and wide-angle reflection profiles, gravimetric modeling, receiver function studies and seismic tomography (e.g. Aljinović, 1983, Skoko et al., 1987, Orešković et al., 2011, Stipčević et al., 2011, Šumanovac et al., 2009, Šumanovac, 2010). Although these studies documented the general layout of the Moho in this region most of them had available either a limited number of data points or had a low resolution in the crucial areas where Moho depth changes rapidly. Here we present crustal thickness map (Fig. 5) based on the analysis of teleseismic P-wave crustal conversions for a large number of stations in the Dinarides. Using data from temporary seismic stations deployed within AlpArray and AlpArray-CASE allowed us to interpolate on relatively short distances (usually to less than 50 km – see Fig. 5) and to probe areas previously not covered by seismic experiments. In the following we will discuss our measurements in the context of previous findings and implications that these results could have on our understanding of the tectonic evolution of the Dinaric region.

It is broadly accepted that two types of Moho exist below the Dinarides – the Adriatic and significantly shallower Moho originating from Europe-derived units in the Pannonian basin (Tari & Pamić, 1998; Schmid, 2008; Ustaszewski et al., 2008; Handy et al., 2015). Our results confirm this general outline but also add some new insights

about the relationship and interaction between the different units involved. The transition zone between Adriatic and European Moho is well mapped in our RF investigation and confirms sharp change from thick to thinner crust when moving from the External Dinarides to the Internal Dinarides and the Pannonian units (profiles A–C in Fig. 8). On one hand, these values confirm the results of Šumanovac (2010) based on gravity modeling although our measurements favor much deeper Moho (>50 km) under the central-southern Dinarides. On the other hand, in the transition from External Dinarides into the Adria domain, our results suggest a broad zone of relatively thick crust and gradual decrease in Moho depth.

In contrast to the currently prevailing models, we measured the Moho depths in excess of 45 km under the central Adriatic islands. This was hinted in two previous RF studies (van der Meijde et al., 2003 and Stipčević et al., 2011) but only beneath a single station whereas here we find a broad area of thick crust coinciding with the Mid-Adriatic ridge system. In the transition zone and the Pannonian basin, we generally find much shallower crustal thickness values ranging from 25 to 35 km. The uncertainty in Moho depth estimations in these regions is low, generally less than 3 km, and is much smaller compared to the Dinarides-Adriatic region. This is mainly a consequence of simple crustal structure and almost flat Moho boundary. In contrast, crustal structure in the Dinarides is more complex with several marked discontinuities in the crust (*e.g.* carbonate cover and transition from upper to lower crust) and the Moho depth is characterized by strong lateral variations. Furthermore, in the regions with the largest uncertainties (central-southern Dinarides) there is indication (*e.g.* Piromallo & Morelli, 2003; Koulakov et al., 2009; Šumanovac et al., 2017; Belinić et al. 2018) for the double or overlapping Moho. Crustal thickness in these areas may therefore be highly influenced by this disposition and will be investigated in subsequent work. Similarly, complex situation is found in NW Slovenia, in the zone of interaction of the Dinarides, the Alps and Adria, which results in less sharply defined crust, and in turn blurs out the signal from the Moho (see outliers CRNS and GBAS, Figs. 2 and 5).

The most striking feature of this investigation, when compared with previous studies, is the significantly deeper Moho under the southern Dinarides. Our results show crustal thickness in excess of 50 km with peak values around 55 km at two stations (CA02A and CA04A). The results at the stations in this area display high coherence, with a single exception of station KOME (large difference due to a relatively small number of usable RFs and complicated crustal structure). Although the results show high uncertainty in Moho depth estimation for this area (~6 km) the overall agreement indicates a deep crustal root. This may be explained by several factors with our preferred model being flexed Adriatic lithosphere below the southernmost part of the Dinaric mountain chain.

In general, the depth of the seismogenic layer tends to follow the shape of the Moho (Fig. 8), and is clearly constrained to the upper crust. This is especially true for the profiles A, C and D (Figs. 1 and 8). In the central part of the Dinarides crossed by the profile B seismicity is sparse and dispersed in the wide zone possibly reflecting the transition from purely thrust oriented faulting to a more strike-slip oriented one in the northwestern Dinarides. This is evident in the Moho depth profile A where there is no seismic activity in the zone of a relatively deep Moho (profile distance 0 to 100 km) designated as stable Adria with seismicity constrained in the zone of thinning crust (from 100 to 140 km). This implies that most of the interaction between Adria and Europe in this region is localized to a narrow belt with dextral movements. In the same profile shallow seismicity further inland (from 170 to 300 km) in the region with crustal thickness of 25–30 km is associated with reactivation of compressional faulting after cessation of the extension movements due to the opening of the Pannonian basin. To the south the situation is markedly different with seismicity being widely dispersed (profiles C and D), similar to the layout in the profile B but with significantly higher occurrence rates and occasional earthquakes larger then magnitude 6.0. Here, most of the earthquake activity is spread in the wide zone under the External Dinarides underlined with a relatively thick crust (Fig. 1a and profiles C and D) and extending into the Adriatic. Whereas the seismicity in the northern portion is mostly confined to the coast and hinterland overlying the zone where the Moho shallows out, seismic activity in the central Adriatic reaches out well beyond the coast (0 to 100–120 km in profiles C and D) enhancing the notion of separation between the northern and the southern portions of the Adriatic microplate (Oldow et al., 2002; D'Agostino et al., 2008). Furthermore, in comparison with the north Adriatic the seismicity in the upper crust of this region is present on both sides of the presumed deformation front approximated by the zone of thickest crust.

Most of the variation in the *Vp/Vs* values is due to the complex crustal structure created during the subduction/collision processes. This is especially evident in the External Dinarides where the underlying units are topped with thick layer of highly fractured and fluid filled limestone. As we are only modelling the average crustal value of *Vp/Vs,* our results can be highly dependent on conditions in one layer. With this in mind the distribution of the higher *Vp/Vs* values broadly follows the thicker crust under the External Dinarides and the Adriatic domain with the exception of the south Adriatic where we observe significantly lower *Vp/Vs* values. Similarly, in the transition zone we found lower *Vp/Vs* values where the crust becomes thinner. In contrast, in the Pannonian basin high *Vp/Vs* values are indicated where the crustal thickness is below 30 km thus suggesting different crustal structure than in the transition zone.

Overall, we find that our results generally follow the Moho disposition outlined in previous compilations but add several new insights. Most important of them are the thicker crust in the central Adriatic, a deep crustal root in the southern Dinarides and a tightly constrained transition from the deep Dinaric to the shallower Pannonian Moho. Comparison of the Moho depths presented here, and the depths to the

lithosphere-asthenosphere boundary (LAB) as published by Belinić et al. (2018), reveals that deep Moho in the External Dinarides corresponds to LAB depths exceeding 90 km, whereas shallow Moho in the Pannonian basin and in the transition zone towards the Alps (NE Slovenia and NW Croatia) is found where LAB lies shallower, typically above 70 km.

This work presents the results of the first large scale seismic investigation encompassing the whole Dinaric mountain belt and may serve as a good starting point for the future crustal models of the region. Hopefully our results will be updated with additional data from various other regional studies currently in progress, possibly also using novel approaches and methods. In particular, it seems that the H–κ–c algorithm (Li et al., 2019) that uses harmonic corrections for RFs to minimize the influence of dipping Moho as well as of the crustal S-wave anisotropy, could be beneficial in this area of pronounced Moho topography.

Acknowledgments. This study has been supported by the Croatian Science Foundation, grant HRZZ IP 2014-09-9666. The operation of the stations STA, CACV, and KSY is funded by Hrvatska Elektroprivreda (HEP). IM, while employed at Geophysical Institute ETH Zurich, was supported by the Swiss National Science Foundation SINERGIA Project CRSII2-154434/1 (Swiss-AlpArray). All support is gratefully acknowledged. We thank the Tectonics Associate Editor and two anonymous reviewers for their constructive reviews and comments which helped us improve the manuscript.

The waveform data were provided by the number of regional seismic networks along with the data from temporary stations installed within the AlpArray project. The data used in the research can be found at http://www.orfeus-eu.org/data/eida/ website or through request to the regional network operators.

The authors are grateful to the members within the AlpArray Seismic Network Team (www.alparray.ethz.ch): Rafael Abreu, Ivo Allegretti, Maria-Theresia Apoloner, Coralie Aubert, Simon Besançon, Maxime Bès de Berc, Didier Brunel, Marco Capello, Martina Čarman, Adriano Cavaliere, Jérôme Chèze, Claudio Chiarabba, Glenn Cougoulat, Luigia Cristiano, Tibor Czifra, Ezio D'Alema, Stefania Danesi, Romuald Daniel, Anke Dannowski, Anne Deschamps, Sven Egdorf, ETHZ-SED Electronics Lab, Tomislav Fiket, Kasper Fischer, Sigward Funke, Aladino Govoni, Gidera Gröschl, Stefan Heimers, Ben Heit, Davorka Herak, Johann Huber, Dejan Jarić, Petr Jedlička, Hélène Jund, Stefan Klingen, Bernhard Klotz, Petr Kolínský, Josef Kotek, Lothar Kühne, Krešo Kuk, Dietrich Lange, Jürgen Loos, Sara Lovati, Deny Malengros, Christophe Maron, Xavier Martin, Marco Massa, Francesco Mazzarini, Laurent Métral, Milena Moretti, Helena Munzarová, Anna Nardi, Jurij Pahor, Catherine Péquegnat, Florian Petersen, Davide Piccinini, Silvia Pondrelli, Snježan Prevolnik, Roman Racine, Marc Régnier, Miriam Reiss, Simone Salimbeni, Marco Santulin, Werner Scherer, Sven Schippkus, Detlef Schulte-Kortnack, Stefano Solarino, Kathrin Spieker, Angelo Strollo, Bálint Süle, Gyöngyvér Szanyi, Eszter Szűcs, Martin Thorwart, Stefan Ueding,

Massimiliano Vallocchia, Luděk Vecsey, René Voigt, Christian Weidle, Gauthier Weyland, Stefan Wiemer, Felix Wolf, David Wolyniec, Thomas Zieke.

The authors also acknowledge the efforts of the AlpArray-CASE Field Team: Matteo Bagagli, Eduard Kissling, John Clinton, Vesna Šipka, Dejan Jarić, Saša Šikman, Snježan Prevolnik, Simone Salimbeni, Ciriaco D'Ambrosio.

References

Aljinović, B. (1983). Najdublji seizmički horizonti sjeveroistočnog Jadrana, Ph.d. thesis, Univ. Zagreb, 219 pp (in Croatian with English summary).

Aljinović, B., Prelogović, E., & Skoko, D. (1987). New data on deep geological structure and seismotectonic active zones in region of Yugoslavia, *Bollettino di Oceanologia Teorica ed Applicata*, **2**, 77–90.

Ammon, C. (1991). The isolation of receiver effects from teleseismic P waveforms, *Bulletin of the Seismological Society of America*, **81**(6), 2504–2510, doi:10.1029/2005JB004161.

Basili, R., Kastelic, V., Demircioglu, M. B., Garcia Moreno, D., Nemser, E. S., Petricca, P., Sboras, S. P., Besana-Ostman, G. M., Cabral, J., Camelbeeck, T., Caputo, R., Danciu, L., Domac, H., Fonseca, J., García-Mayordomo, J., Giardini, D., Glavatovic, B., Gulen, L., Ince, Y., Pavlides, S., Sesetyan, K., Tarabusi, G., Tiberti, M. M., Utkucu, M., Valensise, G., Vanneste, K., Vilanova, S., & Wössner, J. (2013). The European Database of Seismogenic Faults (EDSF) compiled in the framework of the Project SHARE, (Share - The European Database of Seismogenic Faults). DOI: http://doi.org/10.6092/INGV.IT-SHARE-EDSF

Belinić, T., Stipčević, J., Živčić, M., & AlpArray Working Group (2018). Lithospheric thickness under the Dinarides, *Earth and Planetary Science Letters*, **484,** 229–240.

Bennett, R. A., Hreinsdóttir, S., Buble, G., Bašić, T., Bačić, Z., Marjanović, M., Casale, G., Gendaszek, A. & Cowan, D. (2008). Eocene to present subduction of southern Adria mantle lithosphere beneath the Dinarides, *Geology*, **36**(1), 3, doi:10.1130/G24136A.1.

Bijwaard, H., & Spakman, W. (2000). Non-linear global P-wave tomography by iterated linearized inversion, *Geophysical Journal International*, **141**(1), 71–82, doi: 10.1046/j.1365-246X.2000.00053.x.

Brückl, E., F. Bleibinhaus, A. Gosar, M. Grad, A. Guterch, P. Hrubcová, G. R. Keller, M. Majdański, F. Šumanovac, T. Tiira, J. Yliniemi, E. Hegedűs, & H. Thybo (2007). Crustal structure due to collisional and escape tectonics in the Eastern Alps region based on profiles Alp01 and Alp02 from the ALP 2002 seismic

experiment, *Journal of Geophysical Research*, **112**(B6), B06,308, doi:10.1029/2006JB004687.

Chen, Y., Niu, F., Liu, R., Huang, Z., Tkalčić, H., Sun, L., & Chan, W. (2010). Crustal structure beneath China from receiver function analysis, *Journal of Geophysical Research*, **115**(B03307), 1–22, doi:10.1029/2009JB006386.

Chevrot, S. & van der Hilst, R. (2000). The Poisson ratio of the Australian crust: Geological and geophysical implications, *Earth and Planetary Science Letters*, **183**(1), doi:10.1016/S0012-821X(00)00264-8

D'Agostino, N., Avallone, A., Cheloni, D., D'Anastasio, E., Mantenuto, S., & Selvaggi, G. (2008). Active tectonics of the Adriatic region from GPS and earthquake slip vectors, *Journal of Geophysical Research*, **113**, B12413. https://doi.org/10.1029/2008JB005860

Dragašević, T. (1969). Investigation of the structural characteristics of the Mohorovičić discontinuity in the area of Yugoslavia, *Bollettino di Geofisica Teorica ed Applicata*, **XI** (41–42), 57–69.

Dragašević, T. (1973–1974). Present-day structure of the Earth's crust and the upper mantle on the territory of Yugoslavia. *Vesn. Zavoda Geol. Geof. Istr.*, **XIV/XV**, Ser. C, 41–51 (in Serbian with English abstract).

Dragašević, T. & Andrić, B. (1975). Dosadašnji rezultati ispitivanja građe Zemljine kore dubokim seizmičkim sondiranjem na području Jugoslavije. *Acta Seismologica Iugoslavica*, **2–3**, 47-50 (in Serbian).

Draper, N., & Smith, H. (1998). Applied Regression Analysis, 706 pp., Wiley, Canada.

Grad, M., & Tiira, T. (2012). Moho depth of the European Plate from teleseismic receiver functions, *Journal of Seismology*, **16**, 95–105.

Grad, M., Tiira, T & ESC Working Group (2009). The Moho depth map of the European Plate, *Geophysical Journal International*, **176**(1), 279–292, doi:10.1111/j.1365246X.2008.03919.x.

Handy, M. R., Ustaszewski, K., & Kissling, E. (2015). Reconstructing the Alps–Carpathians– Dinarides as a key to understanding switches in subduction polarity, slab gaps and surface motion, *International Journal of Earth Sciences*, **104**(1), 1–26, doi: 10.1007/s00531-014-1060-3.

Hetényi, G., Molinari, I., Clinton, J., Bokelmann, G., Bondár, I., Crawford, W., Dessa, J., Doubre, C., Friederich, W., Fuchs, F., Giardini, D., Gráczer, Z., Handy, M., Herak, M., Jia, Y., Kissling, E., Kopp, H., Korn, M., Margheriti, L., Meier, T., Mucciarelli, M., Paul, A., Pesaresi, D., Piromallo, C., Plenefisch, T., Plomerová, J., Ritter, J., Rümpker, G., Šipka, V., Spallarossa, D., Thomas, C., Tilmann, F., Wassermann, J., Weber, M, Wéber, Z., Wesztergom, V., Živčić, M., AlpArray Seismic Network Team, AlpArray OBS Cruise Crew, & AlpArray Working Group (2018). The AlpArray Seismic Network – a large-scale European experiment to image the Alpine orogen.

Surveys in Geophysics, **39**, 931832, 25 doi:https://.org/10.1007/s10712-018-9472-4.

Herak, M., Herak, D. & Markušić, S. (1996). Revision of the earthquake catalog and seismicity of Croatia, 1908–1992, *Terra Nova,* **8**, 86–94.

Herak, D. & Herak, M. (1995). Body-wave velocities in the circum-Adriatic region, *Tectonophysics*, **241**, (1-2), 121–141, doi:10.1016/0040-1951(94)00160-B.

Horváth F. (1993). Towards a mechanical model for the formation of the Pannonian basin. *Tectonophysics*, **226**, 333–357.

Horváth, F., Bada, G., Szafian, P., Tari, G., Adam, A. & Cloetingh, S. (2006). Formation and deformation of the Pannonian Basin: constraints from observational data, *Geological Society, London, Memoirs*, **32**(1), 191–206, doi:10.1144/GSL.MEM.2006.032.01.11.

Kapuralić, J., Šumanovac, F., & Markušić, S. (2019). Crustal structure of the northern Dinarides and southwestern part of the Pannonian basin inferred from local earthquake tomography. *Swiss Journal of Geosciences*, **112** (1), 181-198 doi:10.1007/s00015-018-0335-2.

Koulakov, I., Kaban, M. K., Tesauro, M. & Cloetingh, S. (2009). P- and S-velocity anomalies in the upper mantle beneath Europe from tomographic inversion of ISC data, *Geophysical Journal International*, *179*(1), 345–366, doi:10.1111/j.1365301 246X.2009.04279.x.

Langston, C. A. (1977). Corvallis, Oregon, crustal and upper mantle receiver structure from teleseismic P and S waves, *Bulletin of the Seismological Society of America*, **67**(3), 713–724.

Langston, C. A. (1979). Structure under Mount Rainier, Washington inferred from teleseismic body waves, *Journal of Geophysical Research*, **84**, B9, 4749, doi: 10.1029/JB084iB09p04749.

Li, J., Song, X., Wang, P., & Zhu, L. (2019). A generalized H-κ method with harmonic corrections on Ps and its crustal multiples in receiver functions. Journal of Geophysical Research: Solid Earth, **124**, 3782-3801. https://doi.org/10.1029/2018JB016356

Ligorrıa, J. P., & C. J. Ammon (1999). Iterative deconvolution and receiver function estimation, *Bulletin of the Seismological Society of America*, **89**, 1395–1400.

Lombardi, D., J. Braunmiller, E. Kissling, & D. Giardini (2008). Moho depth & Poisson's ratio in the Western-Central Alps from receiver functions, *Geophysical Journal International*, **173**(1), 249–264, doi:10.1111/j.1365-246X.2007.03706.x.

Matenco, L., & D. Radivojević (2012). On the formation and evolution of the Pannonian Basin: Constraints derived from the structure of the junction area

between the Carpathians and Dinarides, *Tectonics*, *31*(6), n/a–n/a, doi:10.1029/2012TC003206.

MedNet project partner institutions: Mediterranean Very Broadband Seismographic Network (MedNet), Istituto Nazionale di Geofisica e Vulcanologia (INGV), Italy, doi:10.13127/SD/fBBBtDtd6q, 1988.

Molinari, I., & A. Morelli (2011). EPcrust: A reference crustal model for the European plate, *Geophysical Journal International*, **185**(1), 352–364.

Molinari, I., Clinton, J., Kissling, E., Hetényi, G., Giardini, D., Stipčević, J., Dasović, I., Herak, M., Šipka, V., Wéber, Z., Gráczer, Z., Solarino, S., & the Swiss-AlpArray Field Team, (2016) Swiss-AlpArray temporary broadband seismic stations deployment and noise characterization. *Advances in Geosciences*, **43**, 15-29 doi::10.5194/adgeo-43-15-2016.

Molinari, I., Dasović, I., Stipčević, J., Šipka, V., Kissling, E., Clinton, J., Salimbeni, S., Prevolnik, S., Giardini, D., Wiemer, S., AlpArray-CASE Field Team, & AlpArray-CASE Working Group (2018). Investigation of the Central Adriatic Lithosphere structure with the AlpArray-CASE seismic experiment. *Geofizika*, **35** (2), 103-128 doi:10.15233/gfz.2018.35.6.

Ogden, C.S., Bastow, I.D., Gilligan, A., and Rondenay, S., (2019) A reappraisal of the H-κ stacking technique: implications for global crustal structure, *Geophysical Journal International*, **219**(3), 1491 -1513, https://doi.org/10.1093/gji/ggz364

Oldow, J. S., Ferranti, L., Lewis, D. S., Campbell, J. K., D'Argenio, B., Catalano, R., Pappone, G., Carmignani, L., Conti, P., & Aiken, C.L.V (2002). Active fragmentation of Adria, the north African promontory, Central Mediterranean orogen. *Geology*, **30**(9), 779–782. https://doi.org/10.1130/0091-7613(2002)030<0779:AFOATN>2.0.CO;2

Orešković, J., F. Šumanovac, & E. Hegedűs (2011). Crustal structure beneath Istra peninsula based on receiver function analysis., *Geofizika*, **28**, 247–263.

Pamić, J. (2002). The Sava-Vardar Zone of the Dinarides and Hellenides versus the Vardar Ocean The Sava-Vardar Zone of the Dinarides and Hellenides versus the Vardar Ocean, *Eclogae Geologicae Helvetiae*, **95**(1), 99–113.

Piana Agostinetti, N., & Amato, A. (2009). Moho depth and Vp / Vs ratio in peninsular Italy from teleseismic receiver functions, *Journal of Geophysical Research*, **114**(B6), B06,303, doi:10.1029/2008JB005899.

Piromallo, C., & A. Morelli (2003). P wave tomography of the mantle under the Alpine-Mediterranean area, *Journal of Geophysical Research*, **108**(B2), 2065, doi: 10.1029/2002JB001757.

Ratschbacher, L., Merle, O., Davy, P., & Cobbold, P. (1991a). Lateral extrusion in the Eastern Alps; part 1: Boundary conditions and experiments scaled for gravity, *Tectonics*, **10**, 2, 245–256.

Ratschbacher, L., Frisch, W., Linzer, H.G., & Merle, O. (1991b). Lateral extrusion in the Eastern. Alps; part 2: Structural analysis, *Tectonics*, **10**, 2, 257–271.

Rychert, C. A., & Harmon, N. (2016). Stacked *P*-to-*S* and *S*-to-*P* receiver functions determination of crustal thickness, V_p, and V_s: The *H*-*V* stacking method, *Geophysical Research Letters*, **43**, 1487–1494, doi:10.1002/2015GL067010.

Sambridge, M. (1999). Geophysical inversion with a neighbourhood algorithm-I. Searching a parameter space, *Geophysical Journal International*, **138**(2), 479–494, doi: 10.1046/j.1365-246X.1999.00876.x.

Schmid, S. M., Bernoulli, D., Fügenschuh, B., Matenco, L., Schefer, S., Schuster, R., Tischler, M. & Ustaszewski, K. (2008). The Alpine-Carpathian-Dinaridic orogenic system: correlation and evolution of tectonic units, *Swiss Journal of Geosciences*, **101**(1), 139–183, doi:10.1007/s00015-008-1247-3.

Skoko, D., Prelogović, E. & Aljinović, B. (1987). Geological structure of the Earth's crust above the Moho discontinuity in Yugoslavia, *Geophysical Journal International*, **89**(1), 379–382, doi:10.1111/j.1365-246X.1987.tb04434.x.

Stipčević, J., Tkalčić, H., Herak, M., Markušić, S. & Herak, D. (2011). Crustal and uppermost mantle structure beneath the External Dinarides, Croatia, determined from teleseismic receiver functions, *Geophysical Journal International*, **185**(3), 1103–1119, doi:10.1111/j.1365-26X.2011.05004.x.

Subašić, S., Prevolnik, S., Herak, D., & Herak, M. (2017). Observations of SKS splitting beneath the Central and Southern External Dinarides in the Adria-Eurasia convergence zone, *Tectonophysics*, **70**, 593–100.

Šumanovac, F., Orešković, J. & Grad, M. (2009). Crustal structure at the contact of the Dinarides and Pannonian basin based on 2-D seismic and gravity interpretation of the Alp07 profile in the ALP 2002 experiment, *Geophysical Journal International*, **179**(1), 615–633, doi:10.1111/j.1365-246X.2009.04288.x.

Šumanovac, F. (2010). Lithosphere structure at the contact of the Adriatic microplate and the Pannonian segment based on the gravity modelling, *Tectonophysics*, **485**(1-4), 94–106, doi:10.1016/j.tecto.2009.12.005.

Šumanovac, F. & Dudjak, D. (2016) Descending lithosphere slab beneath the Northwest Dinarides from teleseismic tomography. *Journal of geodynamics*, **102**, 171-184 doi:10.1016/j.jog.2016.09.007.

Šumanovac, F., Markušić, S., Engelsfeld, T., Jurković, K., & Orešković, J. (2017). Shallow and deep lithosphere slabs beneath the Dinarides from teleseismic tomography as the result of the Adriatic lithosphere downwelling. *Tectonophysics*, **712/713**, 523–541 doi:10.1016/j.tecto.2017.06.018.

Tari, V., & Pamić, J. (1998). Geodynamic evolution of the northern Dinarides and the southern part of the Pannonian Basin, *Tectonophysics*, **297**, 1-4; 269-281

Ustaszewski, K., Schmid, S. M., Fügenschuh, B., Tischler, M., Kissling, E. & Spakman, W. (2008). A map-view restoration of the Alpine-Carpathian-Dinaridic system for the Early Miocene, *Swiss Journal of Geosciences*, 101(S1), 273–294, doi:10.1007/s00015008-1288-7.

Ustaszewski, K., Kounov, A., Schmid, S. M., Schaltegger, U., Krenn, E., Frank, W. & Fügenschuh, B. (2010). Evolution of the Adria-Europe plate boundary in the northern Dinarides: From continent-continent collision to back-arc extension, *Tectonics*, **29**(6), TC6017, doi:10.1029/2010TC002668.

van der Meijde, M., van der Lee, S., & Giardini, D. (2003). Crustal structure beneath broad-band seismic stations in the Mediterranean region, *Geophysical Journal International*, 152(3), 729–739, doi:10.1046/j.1365-246X.2003.01871.x.

van Gelder, I.E., Willingshofer, E., Sokoutis, D., & Cloetingh, S.A.P.L. (2017). The interplay between subduction and lateral extrusion: A case study for the European Eastern Alps based on analogue models, *Earth and Planetary Science Letters,* **472**, 82–94.

van Unen, M., Matenco, L., Nader, F. H., Darnault, R., Mandic, O., & Demir, V. (2019). Kinematics of foreland-vergent crustal accretion: Inferences from the Dinarides evolution, *Tectonics*, **38**, 49–76, doi.org/10.1029/2018TC005066

Vinnik, L. P. (1977). Detection of waves converted from P to SV in the mantle, *Physics of the Earth and Planetary Interiors*, **15**(1), 39–45, doi:10.1016/0031-9201(77)90008-5.

Wortel, M. J., & Spakman, W. (2000). Subduction and slab detachment in the Mediterranean-Carpathian region., *Science* (New York, N.Y.), 290(5498), 1910–1917, doi:10.1126/science.290.5498.1910.

Yuan, X., Kind, R., Li, X. & Wang, R. (2006). The S receiver functions: synthetics and data example, *Geophysical Journal International*, 165(2), 555–564, doi:10.1111/j.1365246X.2006.02885.x.

Zandt, G., & C. J. Ammon (1995). Continental crust composition constrained by measurements of crustal Poisson's ratio. *Nature*, **374**, 152–154.

Zhu, L. & Kanamori, H. (2000). Moho depth variation in southern California from teleseismic receiver functions, *Journal of Geophysical Research: Solid Earth*, 105(B2), 2969–2980, doi:10.1029/1999JB900322.

Zhu, H., Bozdağ, E., Peter, D., & Tromp, J. (2012). Structure of the European upper mantle revealed by adjoint tomography, *Nature Geoscience*, **5**, 493–498

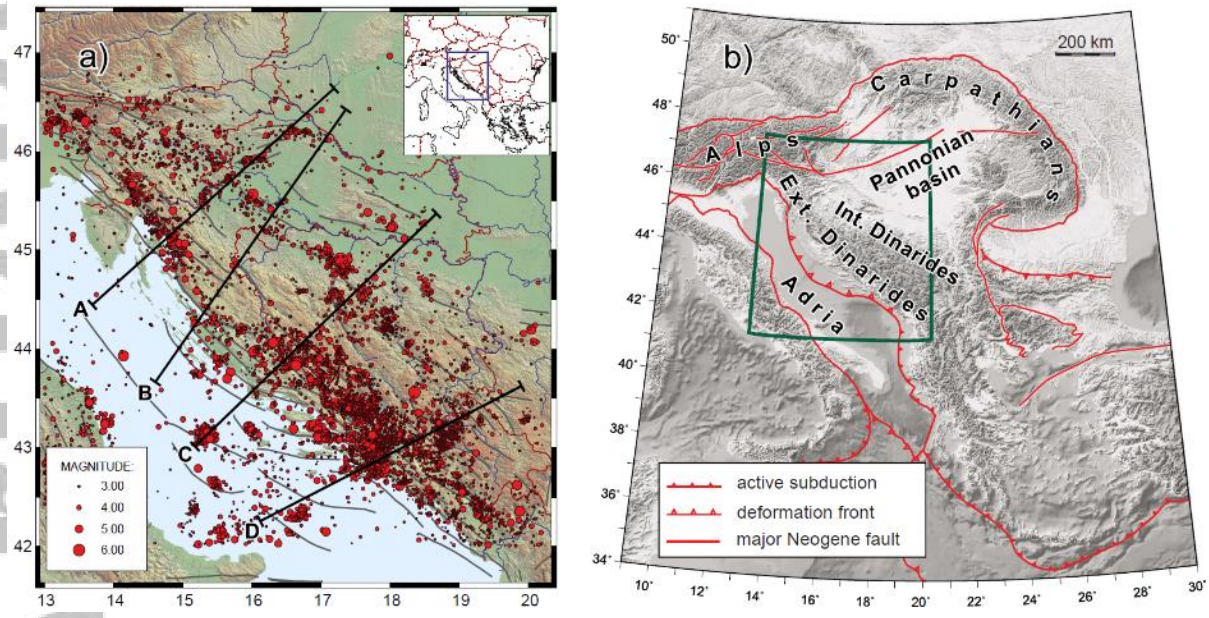

Figure 1. Seismicity and main tectonic provinces in the studied region. (a) Epicenters are from the Croatian Earthquake Catalogue (Herak et al., 1996, last updated on April 2018). Only the events located using at least 20 phase picks are shown. Four lines (A–D) indicate the cross-sections shown in Fig. 8. The surface projections of fault traces from the SHARE project (Basili et al., 2013) are shown as thin gray lines. The region presented is bound by a green rectangle in part b). (b) Tectonic provinces along with the main front lines in and around the investigated region (adapted from Schmid et al. 2008).

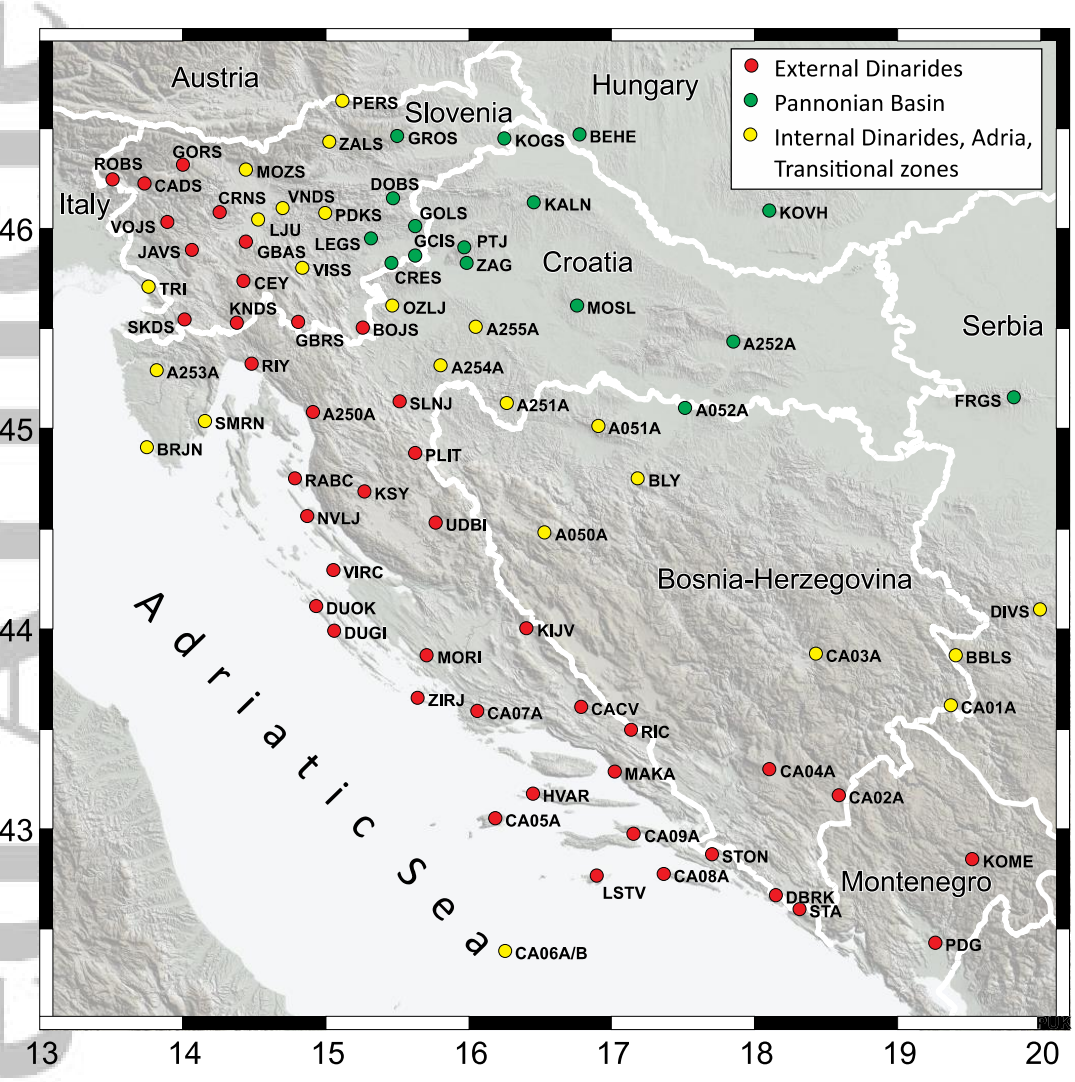

Figure 2. Stations used in the study, colour-coded by the tectonic province.

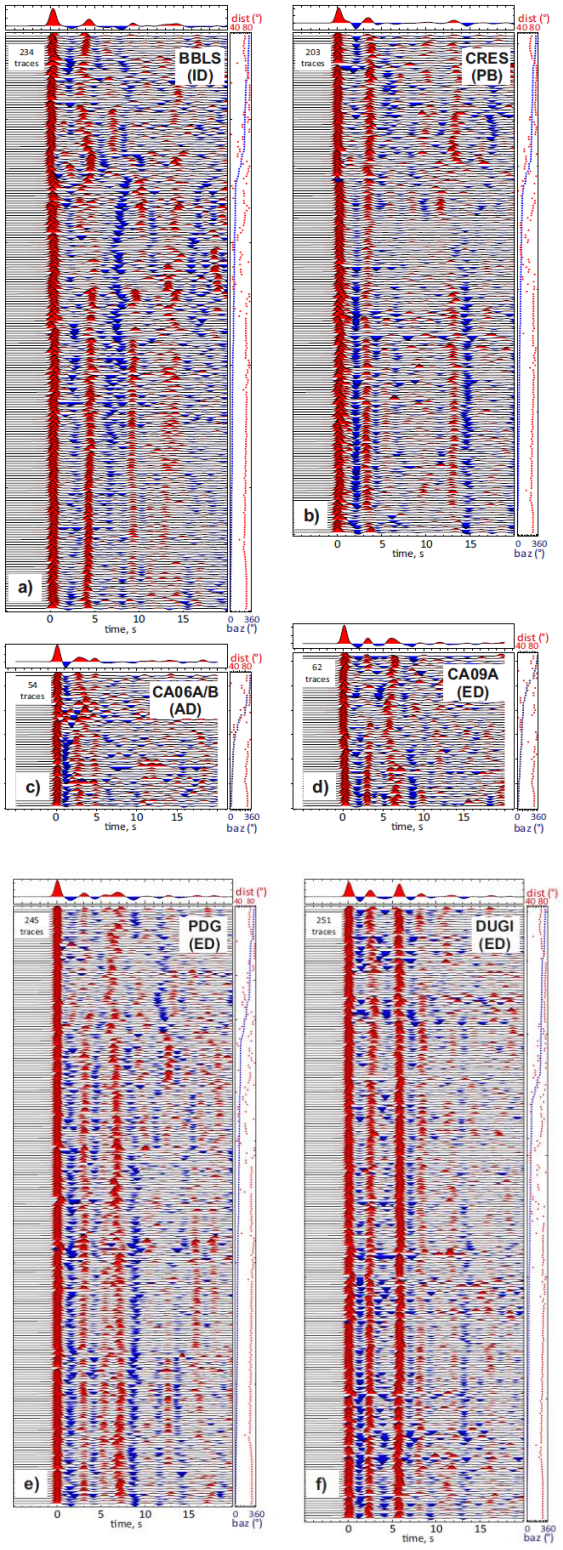

Figure 3. Examples of PRF stacks for six stations in different domains: PB – Pannonian Basin, ID – Internal Dinarides, AD – Adria, ED – External Dinarides (see Fig. 2). The topmost trace is the stack of all observed PRFs, which are ordered bottom-to-top by increasing backazimuth. Positive amplitudes (in red) signify velocity increase with depth while negative amplitudes (in blue) mark velocity decrease with depth. Largest positive

amplitude at time 0 s is the arrival of the main P-wave while other later arriving signals can be related to various velocity discontinuities.

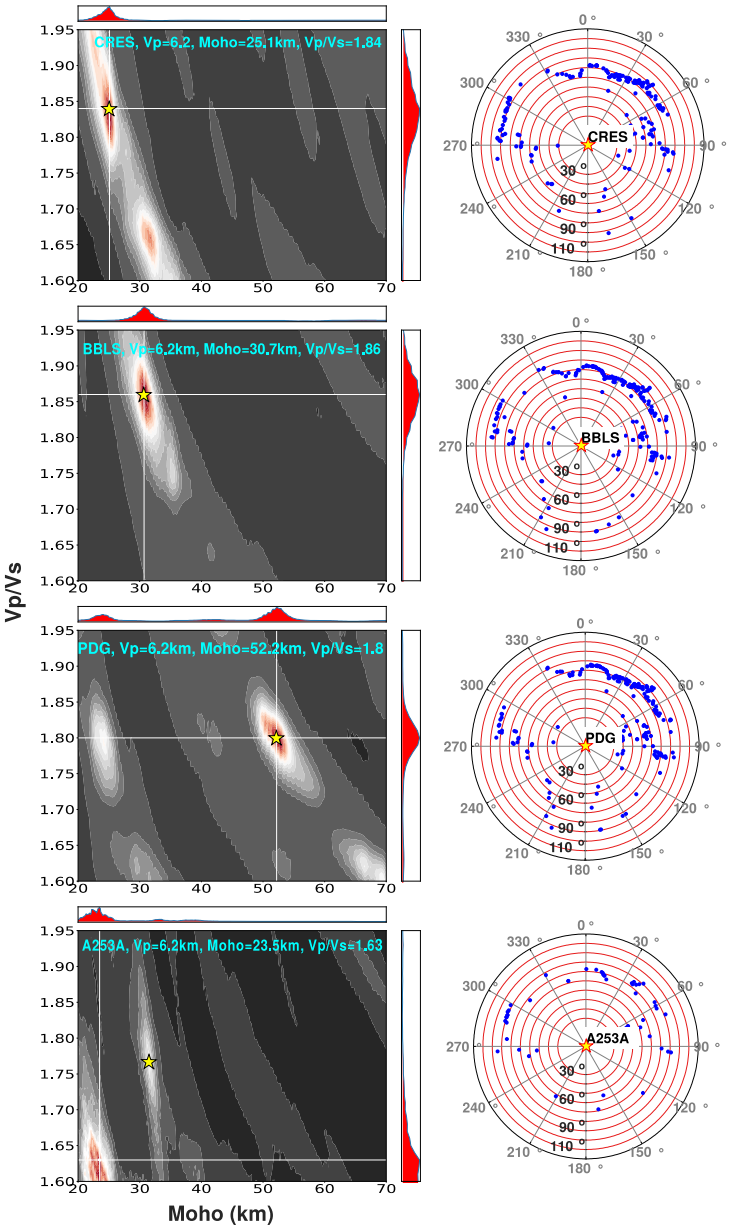

Figure 4. Examples of *H*–*κ* stacking for four stations with different crustal structure. *H*–*κ* stacks (with *H* on the horizontal and *κ* = *Vp/Vs* ratio on the vertical axes) are shown in the left column along with the *H* and *κ* values taken at the maximum value of the stack (intersection of white lines). Yellow star in the *H*–*κ* stacking image on the left denotes our preferred (*H*, *κ)* pair values (see text for details). *H* varied from 20 km to 70 km and *κ* from 1.60 to 1.95, irrespectively of the station's tectonic province. Right column shows backazimuth and distance of the events used in the corresponding *H*–*κ* stack (blue dots).

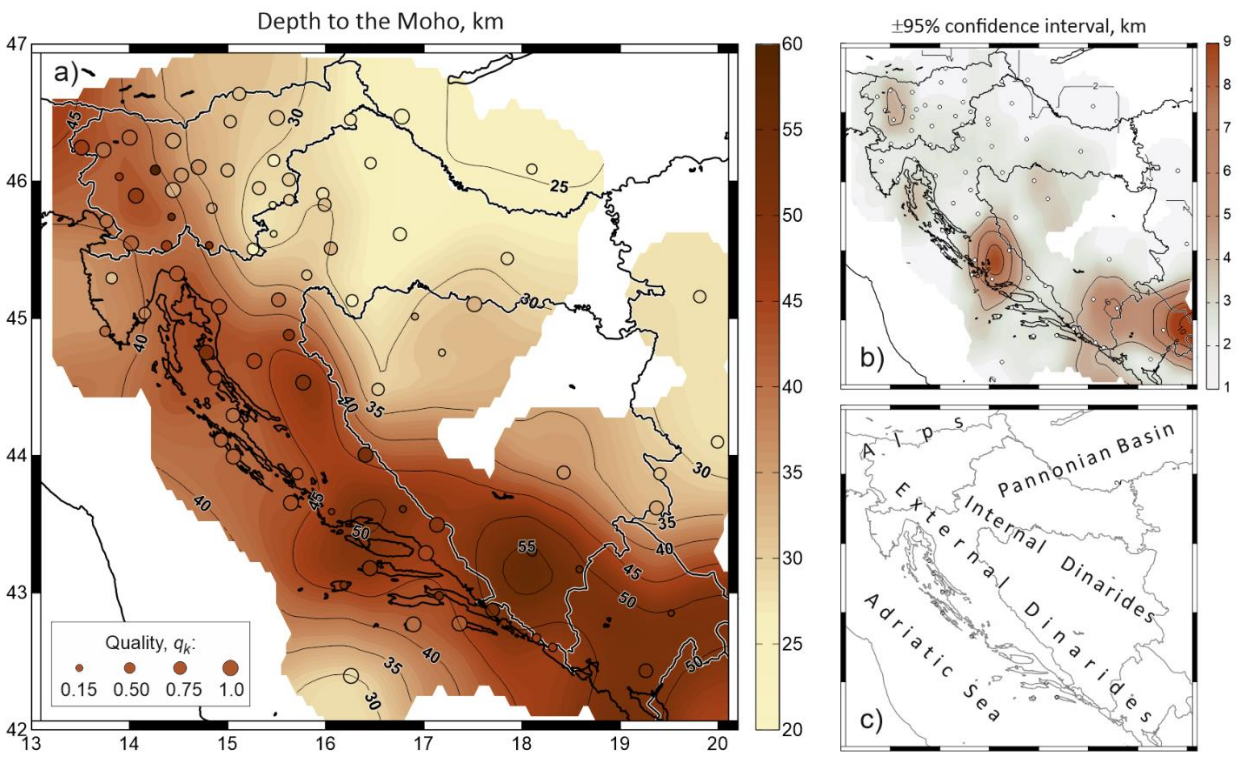

Figure 5. a) Depth (in km) to the Mohorovičić discontinuity below each of the stations is shown by the coloured circles according to the colour scale on the right. The station symbol size is scaled by the corresponding quality of the H–κ estimate, q_k. The interpolated Moho-surface was spatially smoothed with a smoothing kernel of the radius of 41.5 km. **b)** 95%-confidence intervals $CI_{H\varphi\lambda}$ (in km). See text for more detail. **c)** Tectonic domains.

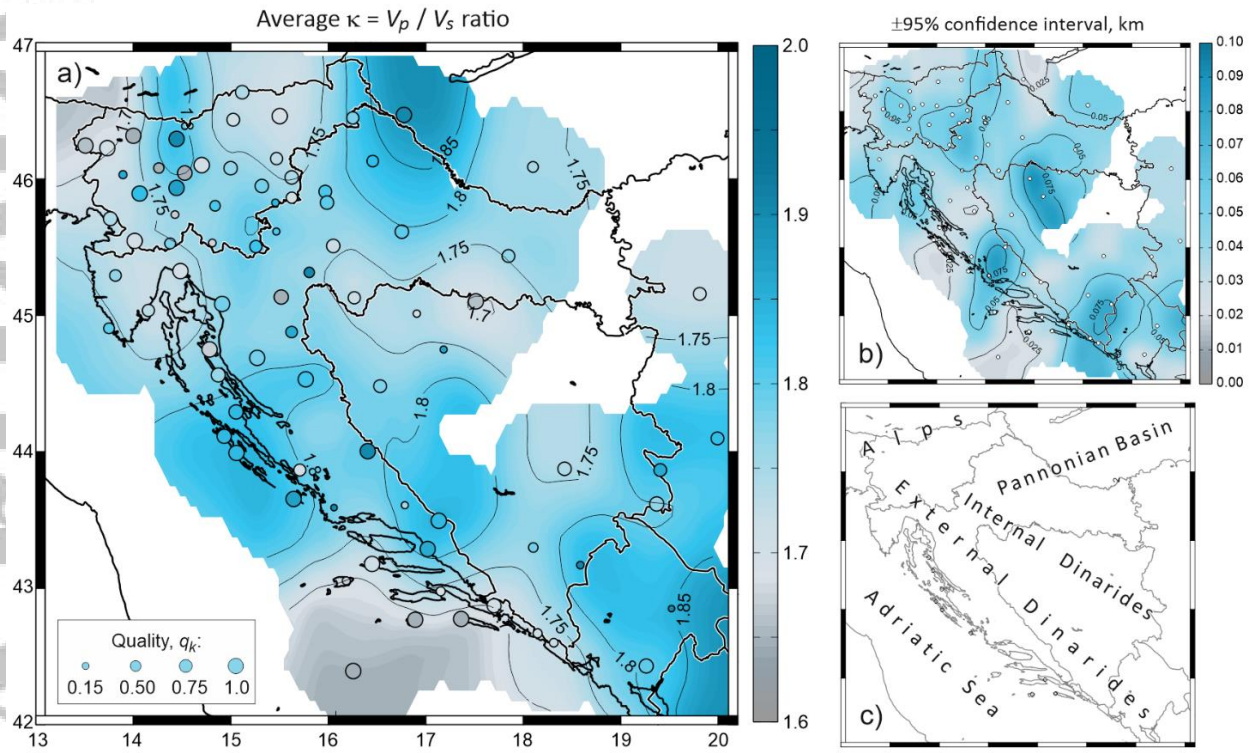

Figure 6. a) Average $\kappa = Vp/Vs$ ratio in the crust below each of the stations is shown by the coloured circles according to the colour scale on the right. The station symbol size is scaled by the corresponding quality of the $H-\kappa$ estimate, q_k. The interpolated Moho-surface was spatially smoothed with a smoothing kernel of the radius of 41.5 km. b) 95%-confidence intervals $CI_{\kappa\varphi\lambda}$. See text for more detail. **c)** Tectonic domains.

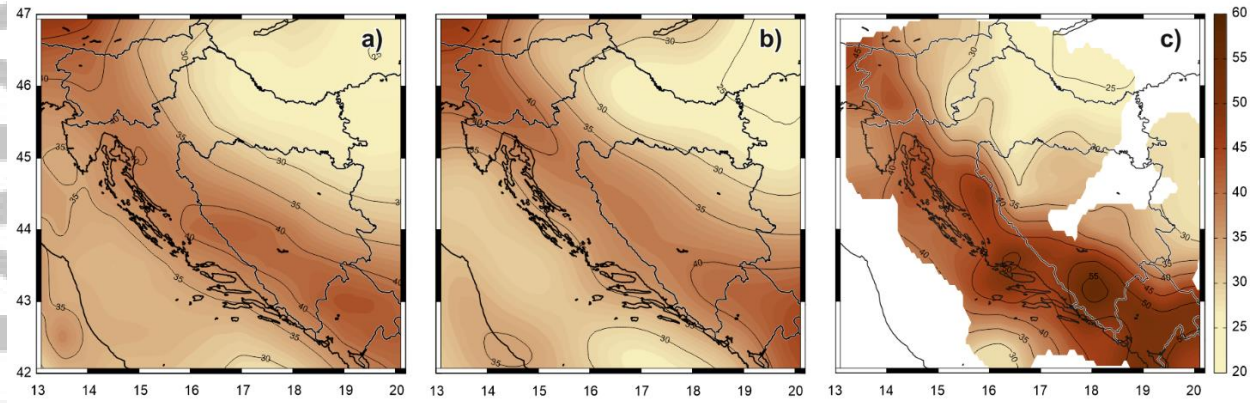

Figure 7. Moho-depth maps for the greater region of the Dinarides. a) EPcrust (Molinari & Morelli, 2011), b) Grad et al. (2009), c) this study.

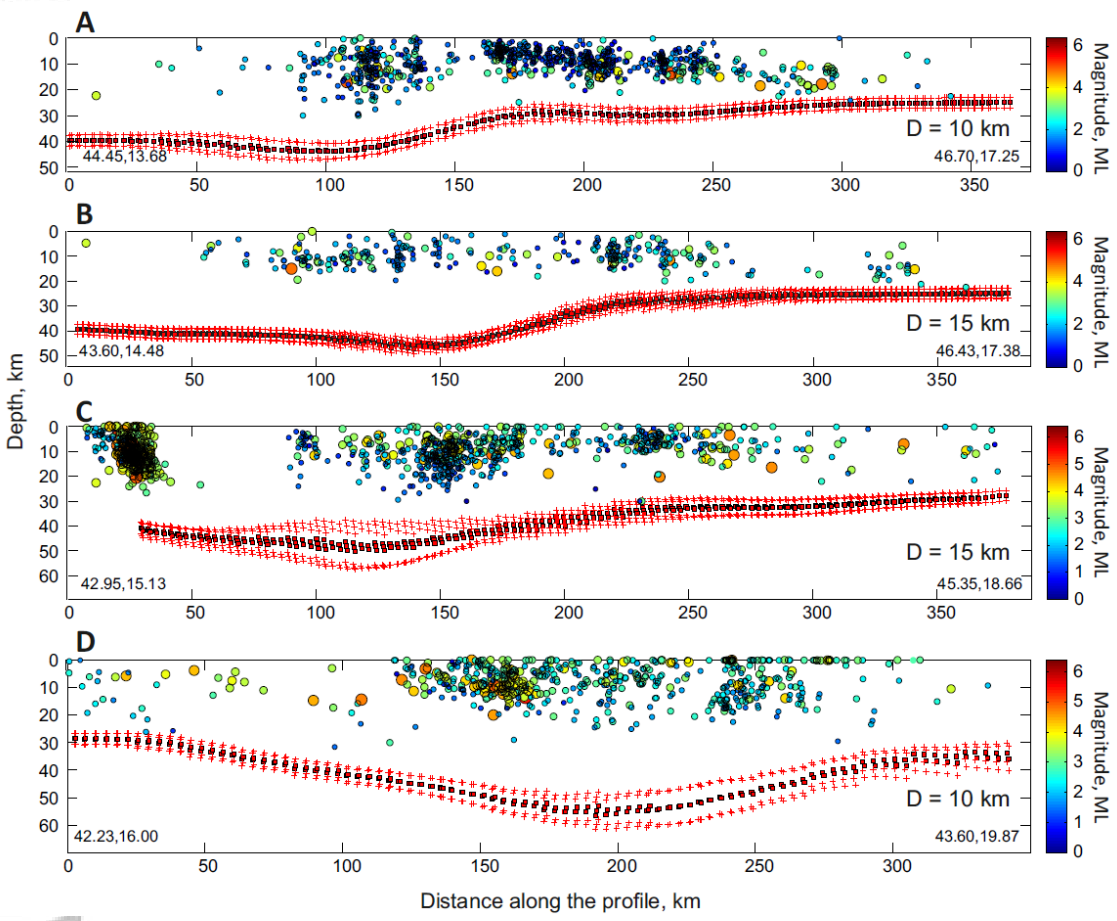

Figure 8. Cross-sections A–D (see Fig. 1 for location). Hypocentres (1908–2017, from the Croatian Earthquake Catalogue, updated version described in Herak et al., 1996), are colour-coded by magnitude and are projected onto the profile from a corridor *D* km wide on each side. Only events located with at least 20 phase arrivals are shown. Mean estimated Moho depths within the corridor are shown by small red squares, red '+' symbols show the confidence interval $CI_{H\varphi\lambda}$. No vertical exaggeration.